Heliyon 10 (2024) e35825

Contents lists available at ScienceDirect

Heliyon

journal homepage: www.cell.com/heliyon

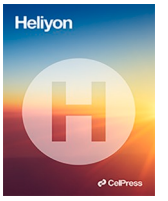

Research article

Biosynthesis and characterization of gold nanoparticles from citrullus colocynthis (L.) schrad pulp ethanolic extract: Their cytotoxic, genotoxic, apoptotic, and antioxidant activities

Abbas Talebi Tadi [a,1], Masoumeh Farhadiannezhad [a,1,2], Maryam Sadat Nezamtaheri [b], Bahram Goliaei [b], Azin Nowrouzi [a,*]

[a] Department of Clinical Biochemistry, School of Medicine, Tehran University of Medical Sciences, Tehran, Iran
[b] Laboratory of Biophysics and Molecular Biology, Department of Biophysics, Institute of Biochemistry and Biophysics, University of Tehran, Tehran, Iran

ARTICLE INFO

Keywords:
Citrullus colocynthis
Cytotoxicity
Genotoxicity
Gold nanoparticles
Antioxidant activity
Green synthesis

ABSTRACT

The age-old discipline of plant therapy has gained renewed importance through the utilization of plants for the synthesis of metal nanoparticles. However, toxicity testing and characterization of the recently synthesized nanomaterials are essential to evaluating their appropriate application. *Citrullus colocynthis* is a medicinal plant with several health benefits. Herein, we used its ethanolic pulp extract (PE) to manufacture gold nanoparticles (PE-AuNPs). Various approaches were employed to assess the MTT_{50} and NR_{50} values of PE and PE-AuNPs at different concentrations in the human hepatocarcinoma cell line (HepG2). The study aimed to assess the genotoxic effects and in vivo toxicity of PE and PE-AuNPs at MTT_{50} dosages. The quasi-spherical, cubic/triangular prisms, and nail-looking particles exhibited no antioxidant properties. They had an absorbance peak between 540 and 560 nm, diameters of less than 20 nm, hydrodynamic diameters of 177.9 nm, and a negative surface charge (−10.3 mV). The significant role of plant phytochemicals in the formation of metal nanoparticles is confirmed by the diminished antioxidant capacity of extract residues following PE-AuNP synthesis. PE-AuNPs exhibited in vivo and cytotoxic effects at relatively lower concentrations compared to PE. In contrast to PE, PE-AuNPs exhibited lower genotoxic at MTT_{50} dosages. Despite having MTT_{50} values of approximately 1.95 ± 0.06 and 0.89 ± 0.03 mg/ml, PE and PE-AuNPs can still be considered biocompatible. Nonetheless, our results suggest that the characteristics of recently produced nanoparticles can differ from those of the matching plant. Further investigation can provide a better understanding of the possible therapeutic and pharmacological impacts of PE-AuNPs.

1. Introduction

Nanotechnology, a field that focuses on particles with sizes ranging from 1 nm to 100 nm, is highly favored in modern sciences due

* Corresponding author.
E-mail addresses: a-talebit@alumnus.tums.ac.ir (A. Talebi Tadi), m-Farhadiannezhad@alumnus.tums.ac.ir (M. Farhadiannezhad), ms_nezamtaheri@ut.ac.ir (M.S. Nezamtaheri), goliaei@ut.ac.ir (B. Goliaei), anowrouzi@tums.ac.ir (A. Nowrouzi).
[1] Abbas Talebi Tadi and Masoumeh Farhadiannezhad contributed equally to this work.
[2] Present address: Department of Clinical Biochemistry, Faculty of Medicine, Hormozgan University of Medical Sciences, Bandar Abbas, Iran.

https://doi.org/10.1016/j.heliyon.2024.e35825
Received 24 January 2024; Received in revised form 2 August 2024; Accepted 5 August 2024
Available online 8 August 2024

to its extensive range of applications [1]. Nanotechnology is expected to bring about substantial technical advancements in the current century [2]. Nanoparticles (NPs) can be produced using three primary methods: physical and chemical techniques, which are widely used but require a significant amount of energy and involve hazardous additives. On the other hand, the biological method, also known as green synthesis, is a one-step process that is quick, simple, cost-effective, environmentally friendly, and highly stable [3].

Metal nanoparticles (MNPs) are employed in several applications such as catalysis, molecular sensing, diagnosis, and disease therapy owing to their distinctive physicochemical and biological characteristics [4]. These characteristics encompass their diminutive dimensions, akin to cellular structures and organelles, expansive surface area that allows for multiple functional groups to be attached [5], the ease of their interaction with receptors, proteins, and nucleic acids [6], and their capacity to be excreted through urine and feces due to their small size [7]. Gold nanoparticles (AuNPs) have garnered significant attention in recent years as a subset of noble MNPs. This is primarily due to their unique intrinsic characteristics, such as their size tunability, high surface-to-volume ratio, bio-imaging capabilities, favorable biocompatibility, low toxicity, and the potential for surface modification [8]. Concerns have been raised regarding the impact of gold nanoparticles on human health due to their increasing usage [9]. Although they possess utility, data are scarce about their genotoxic potential. AuNPs are commonly perceived as bio-inert; yet, there exists a divergence of findings and viewpoints on the safety and biocompatibility of these nanoparticles. Hence, it is imperative to direct attention towards the toxicity and biocompatibility of AuNPs, as highlighted by Lebedová et al. and Patil et al. [8,10].

Green synthesis of AuNPs by many plants, such as Citrus maxima [11], Allium cepa [12], Piper nigrum [13], Lonicera Japonica [14], Chenopodium murale [15], Crocus sativus [16], barberry [17], Coffea arabica seed [18], and Fenugreek seeds extracts [19] has been reported. Despite the successful production of AuNPs using *Citrullus colocynthis* (*C. colocynthis)* seed aqueous extract [1], insufficient practical support exists regarding the synthesis and cytotoxicity of AuNPs derived from the ethanolic extract of its pulp. The preference for utilizing the pulp extract over the leaf or seed extracts was mostly driven by the difficulties encountered in ethanol extract preparation. The process of isolating chlorophyll from the leaf extract and oils from the seed extract is a relatively difficult task that necessitates thorough manipulation and use of toxic compounds, such as methanol, hexane, and chloroform before the final product is obtained.

Colocynthis (bitter apple), a prominent member of the Cucurbitaceae family, exhibits extensive growth in arid regions spanning North Africa, Asia, the Middle East, and Iran. The plant possesses significant nutritional and therapeutic properties [20,21]. Research has demonstrated that *C. colocynthis* contains a diverse range of biologically active substances, including glycosides, flavonoids, alkaloids, carbohydrates, fatty acids, and essential oils. According to Salma [22], Cucurbitacins are the primary constituent of this particular fruit. Cucurbitacins, tetracyclic triterpenoids with high oxidation levels, are widely distributed in plants and have demonstrated significant inhibitory properties against several cancer cell lines [23]. Both the reducing and stabilizing steps during the creation of nanoparticles entail the participation of these phytochemicals.

Using *C. colocynthis* extracts, researchers have synthesized copper nanoparticles (CuNPs), nickel nanoparticles (Ni-NPs), zinc oxide nanoparticles (ZnONPs), and silver nanoparticles (AgNPs) with promising anticancer and antibacterial effects [2,24–28].

In the current investigation, the ethanolic pulp extract (PE) of *C. colocynthis* was employed to synthesize gold nanoparticles (PE-AuNPs). The particles were subjected to various analytical techniques, including UV-VIS spectroscopy, transmission electron microscopy (TEM), field emission scanning electron microscopy (FESEM), energy-dispersive X-ray spectroscopy (EDS), dynamic light scattering (DLS), zeta potential, X-Ray diffraction analysis (XRD), Fourier-transform infrared spectroscopy (FTIR), coupled differential scanning calorimetry–thermal gravimetric analysis (DSC–TGA), and agarose gel electrophoresis (AGE), after their filtration through a 0.45 μm syringe-driven filter. Next, we conducted a comparative analysis of the cytotoxicity and genotoxicity of PE-AuNPs in relation to the raw extract (PE) in the context of human hepatocarcinoma (HepG2) cells. The selection of HepG2 cells as an experimental model for in vitro toxicological investigations is primarily based on the confirmation from in vivo studies that the liver is the principal location for the accumulation of AuNPs. The findings of our study indicated that PE-AuNPs exhibited higher cytotoxicity, although, at MTT_{50} doses, they demonstrated lower genotoxicity compared to PE.

2. Materials and methods

2.1. Materials

The following chemicals were acquired from Sigma Aldrich (St. Louis, MO, USA): hydrochloroauric acid trihydrate (HAuCl4^{3}3H2O), 3-[4,5-Dimethylthiazol-2yl]-2,5-diphenyltetrazolium bromide (MTT) reagent, low melting point (LMP) agarose, Triton X-100, gallic acid, ferric chloride (FeCl3), and SYBR green dye. The Drechslera dematioidea strain Cytochalasin B was acquired from Sigma Aldrich (Israel). The neutral red (NR) solution was acquired from Sigma Aldrich (Dorset, UK). The Folin-Ciocalteu phenol reagent and 2,4,6-Tri(2-pyridyl)-s-triazine (TPTZ) were obtained from Sigma Aldrich (Switzerland). The compound potassium dichromate (PD) was acquired from Riedel-de Haen, (Seelze Hannover, Germany). PAN-Biotech (Aiden Bach, Germany) provided Penicillin/Streptomycin (Pen/Strep). Gibco (New York, USA) supplied FBS, and fetal bovine serum (FBS), and ROTH (Karlsruhe, Germany) supplied DMSO. The source of acridine orange was Hopkins & Williams Ltd. (Swansea, UK). The normal melting point (NMP) agarose was acquired from Kawsar Biotech (Tehran, Iran). The LDH kit was obtained from Biorexfars (Fars, Iran), while DMEM and 0.25 % trypsin-EDTA were acquired from Bio-Idea (Tehran, Iran). Additional compounds were acquired from Merck (Darmstadt, Germany). The Trypan blue dye was acquired from Alfresco (Solon, USA). HepG3 cells were acquired from the National Cell Bank, Pasteur Institute of Iran. The DLS, zeta potential, TEM, FESEM, SEM-EDS, DSC-TGA, XRD, and FTIR procedures were conducted by the Center for Laboratory Services at Sharif University of Technology, Tehran, Iran. The comet experiment was conducted at the Institute of Biochemistry and Biophysics (IBB) at Tehran University, under the supervision of Dr. Goliaie. The eggs of Artemia salina Leach, also

known as brine shrimp eggs, were acquired from a pet store. The fruits of *C. Colocynthis* (voucher number PMP-3639) were gathered from nearby regions in Shooshtar, Khuzestan, Iran.

2.2. Preparation of ethanolic C. Colocynthis pulp extract (PE)

The fruits were subjected to solar drying, resulting in the easy separation of seeds and rind from the dried fruits. Fruit pulp was pulverized into a fine powder. Approximately 10 g of the powder was immersed in 166 ml of 96 % ethanol. The crude extract was filtered using a Whatman filter No.1 after one week at room temperature. It was then dried in an oven at 37 °C. The crude component (referred to as PE) was measured and preserved at a temperature of −20 °C [29].

2.3. Preparation of PE-AuNPs and analysis using UV–VIS spectroscopy

The study examined several concentrations of PE and $HAuCl_4.3H_2O$ to determine the most effective concentrations for synthesizing PE-AuNPs. To find the ideal PE concentration, we selected a 1 mM gold solution, commonly employed in the literature for the green synthesis of nanoparticles. Various concentrations of PE (1, 3, 6, 9, 12 mg/ml) were combined with a stock solution of HAuCl4 (10 mM) to achieve a final concentration of 1 mM. The mixture was then left undisturbed at room temperature in the dark. UV–VIS spectroscopy was conducted within the wavelength range of 300–700 nm using a PerkinElmer UV/Vis Spectrometer (USA) and photographs of the reaction mixtures were captured at 30-min intervals [30]. Subsequently, the chosen concentration of PE (6 mg/ml) was again employed to choose the optimal concentration of $HAuCl_4.3H_2O$ (from a range of 0.5, 1.0, 2.0, and 4.0 mM final concentrations) based on the absorption spectra. The PE-AuNP reaction mixture (40 ml), filtered through a membrane (0.45 μm), underwent centrifugation at $29703 \times g$ for 40 min. After washing twice with deionized water, the final pellet was either resuspended in deionized water or air-dried for further operations.

2.4. Characterization of PE-AuNPs

2.4.1. Examination of the total polyphenol content (TPC) and total antioxidant content (TAC)

The TPC and TAC contents of PE (1, 3, 6, 9, 12 mg/ml solutions), the collected PE-AuNPs after synthesis and centrifugation, and the resulting supernatants were measured using the Folin-Ciocalteu reagent and ferric reducing antioxidant power (FRAP) test, respectively [30].

2.4.2. Agarose gel electrophoresis (AGE)

PE-AuNPs samples (20 μl) were combined with glycerol in a 1:1 ratio and subsequently applied onto the wells of a 0.8 % agarose gel in a 0.5X TBE buffer solution with a pH of 8.0. The electrophoresis procedure was conducted for 40 min at a voltage of 135 V, utilizing an electrophoretic tank (MupidOne, Japan) that was filled with TBE 1X (pH 8.0) [30].

2.4.3. Analysis of particle size and zeta potential

The nanoparticle suspension was subjected to dynamic light scattering (DLS) technique (Malvern Nano ZS (red badge) ZEN 3600, UK) to determine the particle sizes and size distributions [specifically, the hydrodynamic diameters of the PE-AuNPs and polydispersity index (PDI)] as well as the zeta potential or surface charges [30].

2.4.4. Transmission electron microscopy (TEM), field emission scanning electron microscopy (FESEM), and energy dispersive X-ray spectroscopy (EDS)

A 3-μl droplet of PE-AuNP suspension was placed on a thin carbon supporting foil (TEM grid). After applying a gold coating, the shape, size, arrangement, and microscale surface structure of PE-AuNP suspension were analyzed using TEM (Zeiss EM-900, Germany). Concurrently, SEM was performed for both the PE-AuNP suspension as prepared and the air-dried powder (TESCAN, MIRA 3 LMU). The frequency size distribution was computed using ImageJ program. The EDS analysis was used to characterize the elemental composition of the air-dried sample.

2.4.5. X-ray diffraction (XRD) analysis

A thin layer of PE-AuNPs underwent non-destructive testing - X-ray diffraction from polycrystalline and amorphous materials-2 procedures using PANalytical (XPert PRo MPD) instrument. The scanning range (2θ) spanned between 0.8° and 10°.

2.4.6. Fourier transform infrared spectroscopy (FTIR)

The presence of phytochemicals on the surface of nanoparticles was confirmed by conducting Fourier-transform infrared spectroscopy (FTIR) on the extract, supernatant, and washed nanoparticles. FTIR spectra were recorded using a PerkinElmer Spectrum RX-1 instrument (USA) throughout the frequency range of 4000 to 400 cm^{-1}.

2.4.7. Thermogravimetric analysis (TGA)

Coupled differential scanning calorimetry–thermal gravimetric analysis (DSC–TGA) was carried out using METTLER TOLEDO TGA/DSC 1 apparatus (OH, USA). A 5.70 mg sample of the air-dried PE-AuNP was placed in an alumina holder and subjected to heating under a flow of nitrogen gas (50 ml/min) at a rate of 5 °C/min within a temperature range of 25-800 °C.

2.5. Assessment of toxicity

2.5.1. Assays for MTT, NRU, and LDH

Once the cells were seeded in triplicate (2.5 x10^4 HepG2 cells per well) in low glucose DMEM medium supplemented with 10 % FBS, 100 units/ml penicillin, and 100 μg/ml streptomycin, and allowed to adhere for 24 h at 37 °C in a humidified atmosphere with 5 % CO2, they were synchronized for 72 h by replacing the medium with an FBS-free medium. The complete medium was then introduced to the control cells, while the other cell groups (treatment groups) were separately treated to full media containing different doses of filtered PE (0.5, 1, 2, 4 mg/ml) and PE-AuNPs (0.2, 0.4, 0.8, 1 mg/ml). Cell viability was assessed using the MTT colorimetric test at 24, 48, and 72 h following treatment [30]. After the 24-h exposure period, further tests were conducted, including the neutral red uptake (NRU) assay, following the methodology described by Borenfreund and Puerner [31], and the LDH assay using a Biorexfars LDH assay kit (Iran, Fars).

2.5.2. Trypan blue exclusion test

The cells were cultured at a density of 3 x 10^5 cells per well in a 24-well plate with a total volume of 1 ml. The cells were subjected to MTT_{50} doses of PE and PE-AuNPs (2 and 0.9 mg/ml, respectively) in triplicate for 24 h after adhesion and synchronization. A hemocytometer and the trypan blue dye (0.4 % solution) were employed to manually enumerate the viable cells. According to Nowak et al. [32], the percentage of viability was determined by applying the formula: viable cells % = (total number of viable cells per ml/total number of cells per ml) x 100 %.

2.5.3. The cytokinesis block micronucleus (CBMN) assay

The CBMN assay was conducted according to the protocol outlined by Bigdeli et al. [33]. In a 6-well plate, cells were seeded in triplicate at a density of 1.0 x10^6 cells per well in a total volume of 3 ml. Following adhesion and synchronization, the cells were subjected to MTT_{50} doses of PE and PE-AuNPs (2 and 0.9 mg/ml, respectively) for 24 h. Subsequently, the supernatants were extracted, and the cells were incubated at 37 °C with a concentration of 6 μg/ml of cytochalasin B dissolved in 0.1 % (v/v) DMSO for a minimum of 28 h. The attached cells were subsequently rinsed with cold PBS and subjected to two rounds of fixation using cold methanol and acetic acid (3:1 v/v) for 20 min following harvesting. In the initial fixation process, a dropwise addition of 4 % formaldehyde was employed to preserve the cytoplasm. The preserved cells were placed onto microscopic slides, allowed to dry naturally, and subsequently stained with a 10 % (v/v) Giemsa solution (pH 7.4) for 20 min at ambient temperature. A total of one thousand bi-nucleated cells were selected at random and thereafter examined using a light microscope (Leica, Germany) at a magnification of 40x. The frequency of micronuclei (MNi) in each sample was determined by dividing the number of cells harboring micronuclei (MNi) by the total number of bi-nucleated cells. The control group (untreated cells) represented the cells with spontaneous induction of MNi. The nuclear division index (NDI) was used to construct an additional measure of cytotoxicity. The formula used is [M1 + 2(M2) + 3(M3) + 4(M4)/N]. In this formula, M1-M4 represents the number of cells with 1–4 nuclei, examined in 500 cells (N) for both exposures and controls.

2.5.4. The alkaline comet assays

The alkaline comet assay was conducted following the methodology outlined by Queiroz et al. [34], with some adjustments. Briefly, following the distribution of 3.0 x 10^5 cells per well on 24-well plates and subsequent synchronization, the HepG2 cells were partitioned into four distinct groups. The experiment involved subjecting two groups to MTT_{50} doses of either PE or PE-AuNPs (2.0 and 0.9 mg/ml, respectively) for 24 h. An untreated group was designated as the negative control. A fourth group was subjected to ultraviolet (UV) radiation for 20 min before collecting the cells. Approximately 5.0 x 10^4 cells from each group were collected and placed in a 0.5 % (w/v) pre-warmed LMP agarose solution on a slide pre-coated with a thin coating of 1 % (w/v) NMP agarose. The slides were submerged in a lysis buffer solution (2.5 M NaCl, 0.1 M EDTA, 0.01 M Tris-HCl, and freshly added 1 % (v/v) Triton X-100, pH 10). The immersion process lasted for 1 h at 4 °C. The slides were incubated in a denaturation buffer (0.3 M NaOH and 0.001 M EDTA, pH 13.6) for 30 min at 4 °C. Subsequently, electrophoresis was performed using a fresh electrophoresis buffer with the same composition, at a voltage of 16 V (1 V/cm, 300 mA) for 30 min. The slides were then immersed in a neutralization buffer (0.4 M Tris HCl, pH of 7.5) for 5 min. The slides were treated with a 50 μl solution of SYBR® Green (20 μg/ml) and then examined using a fluorescence microscope (x20). A minimum of 200 comet photos were randomly picked from each group and subsequently analyzed and evaluated using the OpenComet software.

2.5.5. Double staining using acridine orange and ethidium bromide (AO/EB)

The cells are stained for apoptosis in this test [35]. In summary, the HepG2 cells that were not treated and those that were treated for 24 h with MTT_{50} concentrations of PE (2 mg/ml) and PE-AuNPs (0.9 mg/ml) were collected and subjected to three washes with PBS. Subsequently, the cells were stained with 1 ml of cold PBS containing a 40 μl mixture of 1 mg/ml ethidium bromide (EB) and 1 mg/ml acridine orange (AO) (1:1) in the absence of light for 10 min. The fluorescence microscope (Axioskop 2 plus, Zeiss, Germany) was used to assess the cellular morphology.

2.5.6. Assessment of brine shrimp lethality

According to Kapali and Sharma [36], the present study aimed to assess the impact of extracts and nanoparticles on the hatching process of brine shrimp eggs. Brine shrimp eggs weighing 0.01 g were placed in 60 mm plates and submerged in seawater that contained either PE or PE-AuNPs at concentrations of 2.0 and 0.9 mg/ml, respectively. The artificial seawater was generated by adding

11g of sea salt to 500 ml of tap water. Following a 48-h incubation period at ambient temperature, which is the duration necessary for seeds to undergo hatching, and a subsequent 72-h period, the larval count was determined in a 1 ml sample extracted from each plate following agitation to ensure homogeneity. Every dosage underwent two tests, and the counting process was repeated three times. The positive control in this experiment involved potassium dichromate (PD, 0.35 mg/ml), while the negative control consisted of a sample without any medication. The percentage of viability was determined by employing the subsequent formula: Viability = (the number of larvae in 1 ml of test/number of larvae in 1 ml of negative control) × 100 %.

2.6. Statistical analysis

The MTT_{50} and NR_{50} values were obtained using Prism software for data analysis, and the results were reported as Mean ± SD. One-way analysis of variance (ANOVA) was employed, followed by repeated post-hoc comparisons using Tukey's test, to ascertain the p-

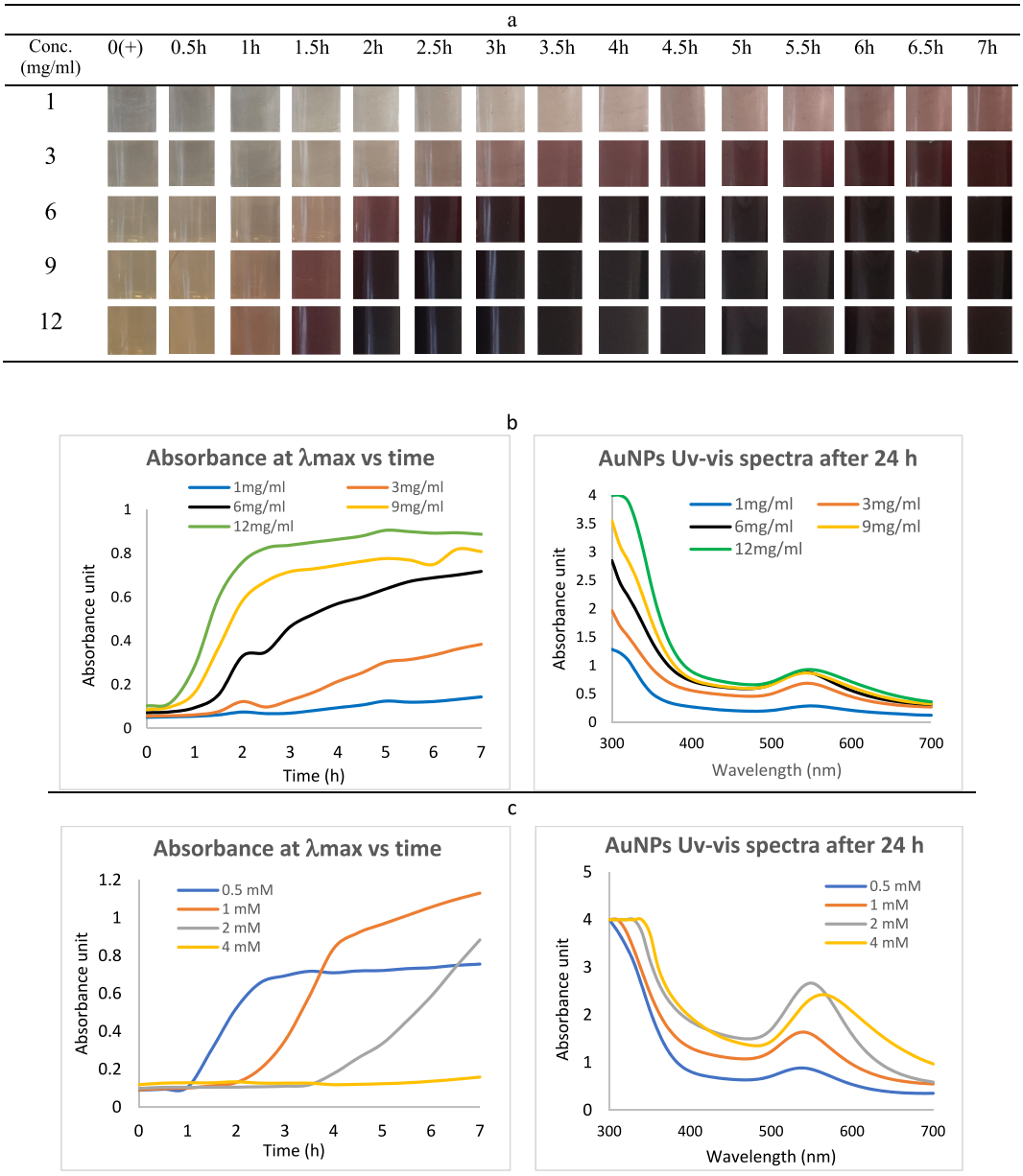

Fig. 1. The absorption kinetics of PE-AuNP synthesis. The color profile (SPR) (a), the absorption maximum profile over time, as well as the UV–vis absorption spectra at different times for the synthesis of PE-AuNP employing varied concentrations of PE (b) and $HAuCl_4.3H_2O$ (c). The term "0 (+)" denotes the initial extract at time zero, which occurs immediately following the introduction of the $HAuCl_4$ solution. (For interpretation of the references to color in this figure legend, the reader is referred to the Web version of this article.)

values that were deemed statistically significant, meaning they were below the threshold of 0.05.

3. Results

3.1. Preparation of extracts from the pulp of C. colocynthis (PE)

A yield of approximately 2.58 ± 0.05 g (25.46 %) of dry material was obtained from 10.0 g of *C. colocynthis* pulp.

3.2. Synthesis of AuNPs using PE

The color change observed in Fig. 1a was a result of the reduction of Au^{3+} ions to Au^0 when the extracts were mixed with the HAuCl4 solution at various concentrations of PE. The color change ranged from pale yellow to various shades of purple, depending on the duration of time elapsed. The synthesis of a limited number of NPs was observed at low concentrations of PE (1 and 3 mg/ml) (Fig. 1b, left and right). Conversely, higher concentrations of PE resulted in the formation of larger particles (as indicated by the redshift of absorption maxima from 540 to 550, Fig. 1b, right). The optimal peak area was achieved at a concentration of 6 mg/ml of PE at the lightest wavelength of 540 nm.

In contrast to the rapid initiation and early stabilization of absorption maxima profiles observed at low concentrations of HAuCl4, higher concentrations of HAuCl4 resulted in a delayed or alternative pathway for the synthesis of PE-AuNP, as depicted in Fig. 1c, left. The gradual production of a significant quantity of bigger particles was seen as the concentrations of gold salt increased (Fig. 1c, right). The wavelength at which the highest absorption occurred (λ_{max}) exhibited an upward trend when the concentrations of both reactants (PE and HAuCl4) rose. The optimal peak at 540 nm was achieved with a concentration of 6 mg/ml of PE and a concentration of 1 mM of gold salt solution. A reaction medium with a volume of 10 ml, comprising 6 mg/ml of PE and 1 mM of gold salt, resulted in the production of approximately 4.5 mg of PE-AuNPs.

3.3. Quantification of total polyphenol (TP) and total antioxidant (TA) levels

The TPC and TAC values for the initial PE at various concentrations and the supernatants after collecting the NPs from the reaction mixture are presented in Table 1, based on GA and Fe^{2+} equivalents. The supernatants exhibited a notable drop in antioxidant capabilities following the production of NP (Suppl. S1). Additionally, the synthesized PE-AuNPs did not demonstrate any antioxidant activity.

3.4. Characterization of particles for PE-AuNPs

3.4.1. Analysis of DLS, zeta potential, and AGE

Suppl. S2 displays the hydrodynamic diameters of PE-AuNPs categorized by intensity, number, and zeta potentials after the filtration process. Table 2 indicates that the particles had hydrodynamic diameters of 177.9 nm and a polydispersity index of around 0.311. The electrophoretic mobility pattern of the PE-AuNPs confirmed the presence of a negative surface charge, measuring −10.3 mV. After being filtered using a syringe-driven filter with a mesh size of 0.45 μm, all PE-AuNPs successfully passed through the gel and gathered in a single band (Suppl. S2).

3.4.2. TEM, FESEM, EDS

The data acquired from the examination of TEM and SEM images (Fig. 2a–e) of PE-AuNP suspension in water as prepared is summarized in (Table 2). The bulk (86 %) of PE-AuNPs exhibited quasi-spherical and hexagonal shapes, with diameters smaller than 20 nm; the chart in Fig. 2f displays the frequency size distribution of the TEM micrographs. The TEM pictures revealed the presence of

Table 1
Total polyphenol content (TPC) and total antioxidant capacity (TAC) for *C. colocynthis* ethanolic pulp extract (PE), the PE-mediated AuNPs (PE-AuNPs) and the supernatant solutions after NP collection.

Sample (mg/ml)	TPC	TAC
	(GAE mg/ml), **(GAE mg/g)**	(Fe^{2+} mM), **(Fe^{2+}mg/g)**
PE (1.0)	0.012 ± 0.00, **(12.0 ± 0.00)**	0.332 ± 0.02, **(18.59 ± 1.12)**
PE supernatant (1.0)	0.004 ± 0.00[a], **(NA)**	0.018 ± 0.01[a], **(NA)**
PE (3.0)	0.032 ± 0.00, **(10.66 ± 0.00)**	1.041 ± 0.07, **(19.43 ± 1.30)**
PE supernatant (3.0)	0.011 ± 0.00[a], **(NA)**	0.400 ± 0.007[a], **(NA)**
PE (6.0)	0.054 ± 0.002, **(9.0 ± 0.33)**	1.946 ± 0.03, **(18.16 ± 0.28)**
PE supernatant (6.0)	0.027 ± 0.00[a], **(NA)**	0.941 ± 0.03[a], **(NA)**
PE (9.0)	0.073 ± 0.001, **(8.11 ± 0.11)**	2.517 ± 0.04, **(15.66 ± 0.24)**
PE supernatant (9.0)	0.044 ± 0.00[a], **(NA)**	1.522 ± 0.01[a], **(NA)**
PE (12.0)	0.122 ± 0.001, **(10.16 ± 0.08)**	3.55 ± 0.04, **(16.56 ± 0.18)**
PE supernatant (12.0)	0.066 ± 0.00[a], **(NA)**	1.846 ± 0.01[a], **(NA)**

[a] , indicate significant differences in comparison to PE and PE supernatant, in each group, respectively; $p < 0.0001$. NA, not applicable.

Table 2
The TEM and SEM sizes and zeta potential of *C. colocynthis* derived PE-AuNPs after filtration.

Weight (mg) in 10 ml reaction media	4.5 ± 0.7
TEM data	
Minimum (d. nm)	2.001
Maximum (d. nm)	55.86
Mean for all NPs (d. nm)	12.41 ± 9.80
NPs <20.0 nm (%)	86.72
Mean for NPs <20.0 (d. nm)	9.04 ± 3.49
SEM data	
Mean diameters (nm)	262.36 ± 68.32
Cubes or pyramids	343.91 ± 272.10
Nails (length)	259.89 ± 107.19
Spheres	
DLS data	
Hydrodynamic d.(nm)	177.9 nm
Zeta potential	−10.3 mV
PDI	0.311

various AuNP forms, such as spheres, rods, triangles, and prisms.

Several nanoparticle morphologies, such as sharp nail-like rods of different lengths and widths, spheres, and cubic or triangular prisms, were found via SEM observations. Fig. 3a displays the surface morphology of the air-dried powder of PE-AuNP, while Fig. 3b provides the elemental composition. The EDS graph provides evidence of carbon, oxygen, chloride, and gold in PE-AuNPs, with atomic percentages of around 83 %, 12.6 %, 0.13 %, and 4.3 %, respectively.

3.4.3. XRD analysis

The XRD spectrum (Fig. 4) confirms the successful formation of pure crystalline PE-AuNPs. All diffraction peaks align with the planes of the face-centered cubic (FCC) structure of gold. The distinctive diffraction peaks corresponding to the crystallographic planes (111), (200), (220), and (311) were identified at specific 2θ values of 38.1°, 44.4°, 64.6°, and 77.8°, respectively. These values align with those found in the reference (code 03-065-2870).

3.4.4. Fourier transform infrared spectroscopy (FTIR)

Phenols, flavonoids, alkaloids, glycosides, saponins, tannins, and terpenoids are present in PE. The extract, supernatant (concentrated five folds), and PE-AuNPs were found to contain alcohols, phenols, phosphine, alkenes, amides, amines, alkanes, aromatics, carboxylic acids, and alkynes, as determined by FTIR analysis (Suppl. S3). The adsorption of phytochemicals on the surface of PE-AuNPs was observed through the presence of vibrations at 3449.01 cm^{-1} for alcohols or phenols, 2360.51 cm^{-1} for phosphine, 1639.98 cm^{-1} for alkenes or amides, 1559.54 cm^{-1} for amines, 1472.49 cm^{-1} for alkanes and aromatics, 1419.14 cm^{-1} for carboxylic acids, and 668.25 cm^{-1} for alkynes. The utilization of phytochemicals in the production of PE-AuNPs served as stabilizing and reducing agents.

3.4.5. TGA analysis

TGA (Fig. 5) revealed a significant and consistent weight loss of approximately 27 % between temperatures of 150 and 471 °C, as indicated by the broad and continuous decline. This weight loss coincided with a notable exothermic reaction observed in the differential scanning colorimetry (DSC) trace. The weight loss seen between 100 °C and 200 °C is likely due to the evaporation of water adsorbed by the capping extract. The significant weight reduction within the temperature range of 250–500 °C can be attributed to the combustion of the thin layer of organic material surrounding the nanoparticles. Furthermore, it is postulated that the degradation of resilient aromatic compounds takes place after reaching 400 °C [37]. At the end of the thermal decomposition process, approximately 68 % of the remaining substance consists of pure AuNPs.

3.5. Assessment of cytotoxicity and genotoxicity

3.5.1. Viability assays using MTT and neutral red uptake (NRU)

In this study, HepG2 cells were subjected to varying concentrations of PE (0.5, 1.0, 2.0, 4.0 mg/ml) and PE-AuNPs (0.2, 0.4, 0.8, 1.0 mg/ml) for 24, 48, and 72 h in the context of MTT experiments. However, for NRU experiments, the treatment duration was limited to 24 h. The extract, regardless of the concentrations employed, resulted in substantial reductions in the percentage of viable cells compared to the untreated cells, with these declines being dependent on both time and dosage ($p < 0.0001$). The toxicity of PE-AuNPs commenced at a concentration of 0.8 mg/ml (Suppl. S4). PE-AuNPs exhibited higher toxicity compared to PE, as indicated by their lower MTT_{50} and NR_{50} values (Table 3).

3.5.2. The LDH assay

The release of LDH by HepG2 cells to the culture media was boosted by a high concentration of PE-AuNPs (1.0 mg/ml). All

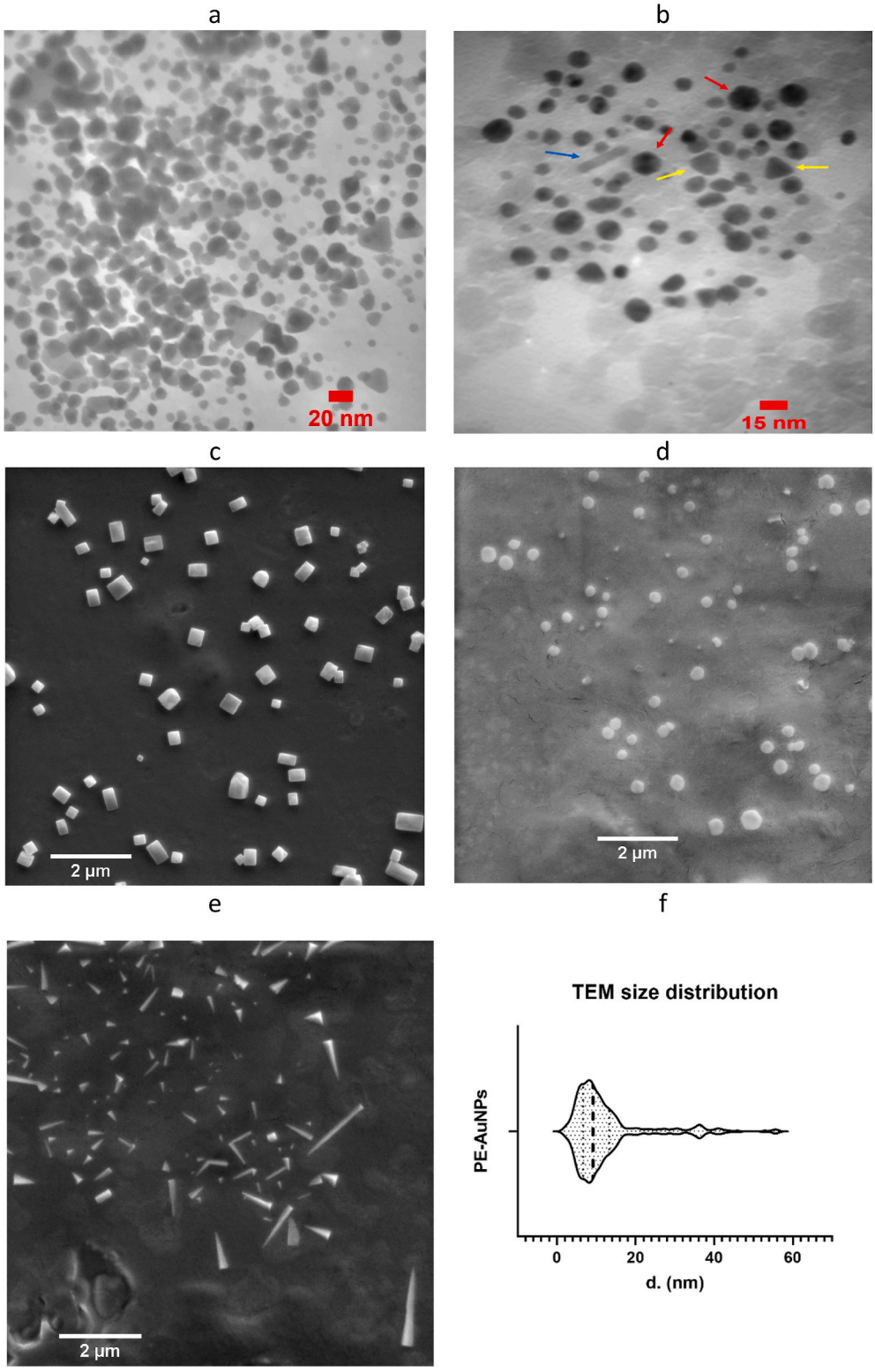

Fig. 2. Two representative transmission electron microscopy (TEM) pictures (a and b), three scanning electron microscope (SEM) images (c–e), and the frequency of size distribution for PE-AuNPs suspension (f). Triangular, rod-shaped, and hexagonal nanoparticles are shown by yellow, blue, and red arrows, respectively. SEM revealed various sizes of different forms of nanoparticles including spherical, cubic, or triangular prisms, and nail-looking spikes with broad flat heads. The images were magnified at 20 000 × . (For interpretation of the references to color in this figure legend, the reader is referred to the Web version of this article.)

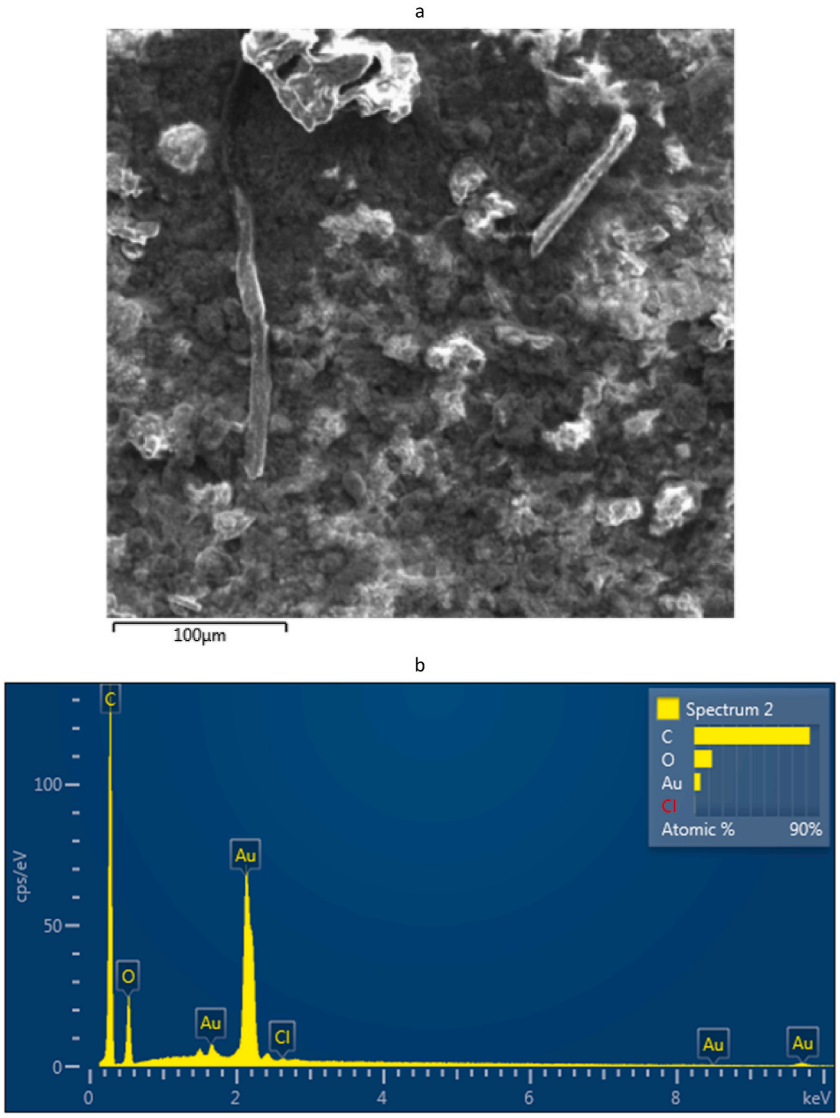

Fig. 3. SEM image (a) and EDS analysis (b) for the powder sample of PE-AuNPs. The SEM image reveals a heterogeneous surface composed of various particles, some elongated and rod-like, while others appear more irregular and rounded.

concentrations of PE were found to be safe. The information was reported as a percentage of the specific activity of the Control (Suppl. S4).

3.5.3. Trypan blue exclusion test

The MTT_{50} doses of PE and PE-AuNPs over 24 h resulted in notable reductions in the percentage of viable cells. Notably, the PE-AuNPs exhibited more cytotoxicity compared to PE, as indicated in Suppl. S4.

3.5.4. Cytokinesis-block micronucleus (CBMN) assay

The untreated cells exhibited a binucleated cell shape, which is characteristic of normal cell division, as evidenced by the presence of micronuclei (MNi) below 2 % (Fig. 6a). Following a 24-h exposure to PE (2.0 mg/ml) and PE-AuNPs (0.9 mg/ml), there was a considerable increase in the number of HepG2 cells with MNi (Fig. 6b).

Furthermore, it was observed that there was a notable rise in mononucleated cells (M1) and a considerable decline in binucleated cells (M2) following exposure to PE and PE-AuNPs at the MTT_{50} concentrations after 24 h (Fig. 6c). The findings of this study suggest that exposure to PE and PE-AuNPs leads to a cytostatic impact. The cytostatic impact of PE and PE-AuNPs on HepG2 cells was confirmed by a considerable drop in the nuclear division index (NDI) for both PE and PE-AuNPs, as shown in Fig. 6d.

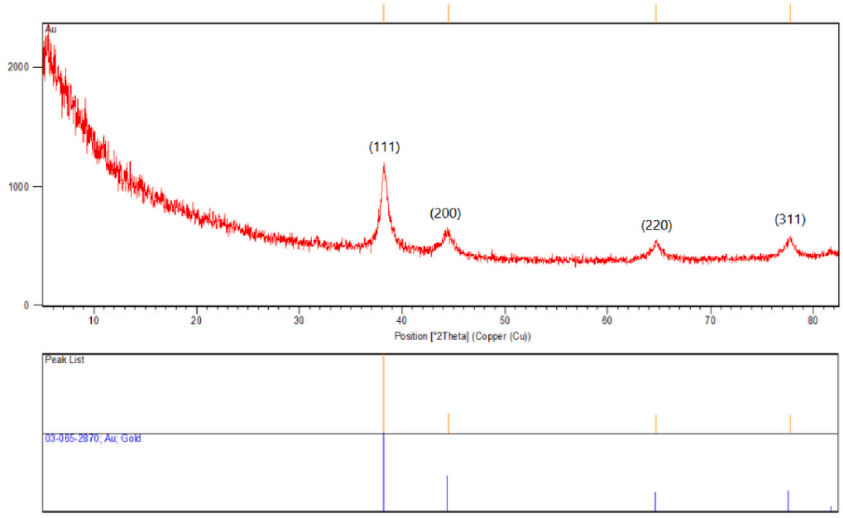

Fig. 4. XRD pattern of face-centered cubic (fcc) structure gold nanoparticles (PE-AuNPs). The peaks are located at 2θ = 38.08°, 44.44°, 64.60°, and 77.72°, and were indexed as (111), (200), (220), and (311), respectively. The reference XRD pattern of Au (JCPDS 03-065-2870) is shown in the lower part. (For interpretation of the references to color in this figure legend, the reader is referred to the Web version of this article.)

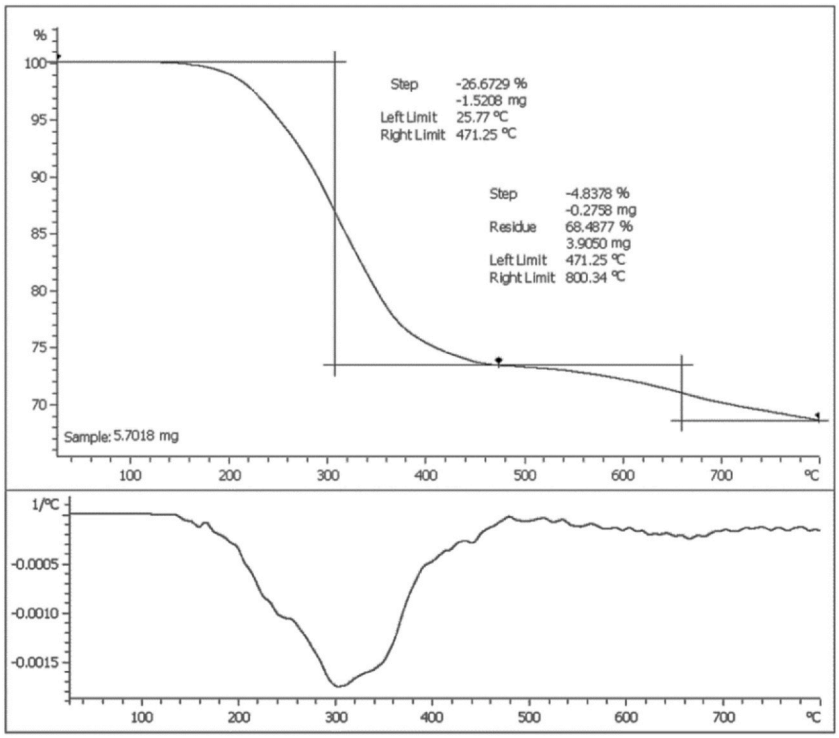

Fig. 5. TGA analysis of dry PE-AuNPs.

3.5.5. Alkaline comet test using single-cell gel electrophoresis

In this study, an alkaline comet assay was conducted to identify DNA strand breaks in HepG2 cells. Following treatment with PE (2.0 mg/ml) and PE-AuNPs (0.9 mg/ml), the analysis of over one hundred fluorescent comets in each group using OpenComet Software (Fig. 7a–d) indicated that the percentage of DNA in the tail (% TD) was 11.18 % ± 10.59 and 8.60 % ± 7.45 for PE and PE-AuNPs, respectively (Fig. 7e). There was a significant difference ($p < 0.0001$) in the %TD of PE and PE-AuNPs compared to the control (3.29 % ± 1.87). The findings of our study are consistent with the documented genotoxic and DNA-damaging effects of AuNPs, as described by Avalos et al. [38]. The %TD value of around 56.5 % ± 22.9 % observed in cells exposed to UV light as a positive control

Table 3
The IC_{50} values calculated from MTT and NRU assays for *C. colocynthis* pulp ethanol extract and the corresponding PE-AuNPs.

IC_{50} (mg/ml)				
	NR_{50}	MTT_{50}		
	24 h	24 h[a]	48 h	72 h
PE	1.72 ± 0.03	1.95 ± 0.06	0.73 ± 0.03	0.76 ± 0.03
PE-AuNPs	0.71 ± 0.04	0.89 ± 0.03	0.56 ± 0.04	0.53 ± 0.04

[a] Note: The 24 h MTT_{50} concentrations of PE and PE-AuNPs (2.0 mg/ml and 0.9 mg/ml, respectively) were used for trypan blue, micronucleus, comet, AO/EB, and shrimp assays.

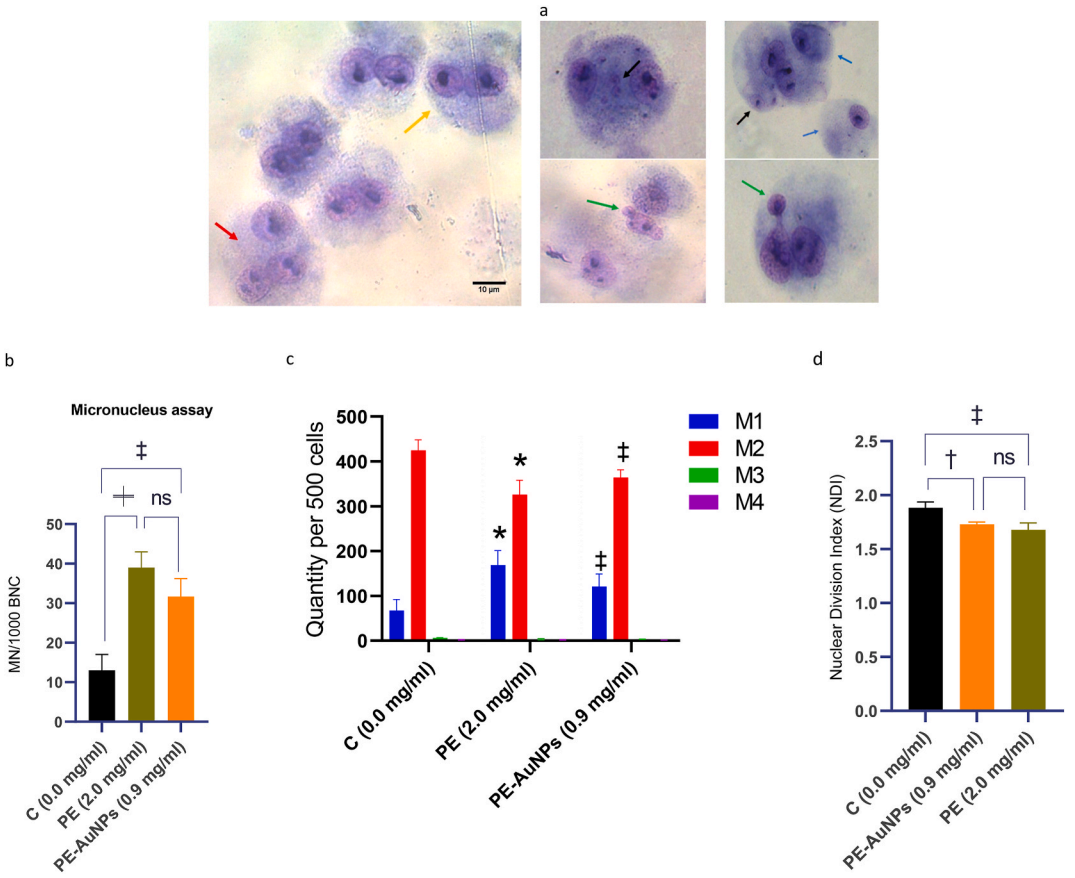

Fig. 6. Micronucleus assay. The microscopic images with blue, yellow, red, green, and black arrows depict various cell types, namely mononuclear, binucleate, trinucleate, and binucleate cells with Mni and buds, respectively (a). Additionally, the frequency of MNi per 1000 cells (b), the frequency of M1-M4, the cell number containing 1–4 nuclei per 500 cells (c), and the NDI (d) are also depicted. The nuclear division index (NDI) is calculated using the formula [M1 + 2(M2) + 3(M3) + 4(M4)/N], where N represents the total number of cells, which is 500. †, $p < 0.05$; ‡, $p < 0.01$; ǂ, $p < 0.001$; *, $p < 0.0001$ compared to control (C). The data is reported as the mean ± standard deviation of three studies. The magnification is 40 × . (For interpretation of the references to color in this figure legend, the reader is referred to the Web version of this article.)

(Fig. 7d) indicates that the comet assay process was conducted correctly.

3.5.6. *Fluorescent labeling as a method for assessing apoptosis*

Representative images and the percentage of cells in each stage of apoptosis are presented in Fig. 8 and Table 4, respectively. Significant reductions in the proportion of healthy non-apoptotic cells were observed as a result of a 24-h exposure to PE (2.0 mg/ml) and PE-AuNP (0.9 mg/ml), which induced a shift towards early apoptosis. PE resulted in a greater proportion of late apoptosis compared to PE-AuNPs. At the doses employed in this experiment, both PE and PE-AuNPs induced negligible levels of necrosis.

3.5.7. *In vivo lethality assay of brine shrimp*

Fig. 9 demonstrates that the presence of PE (2.0 mg/ml) and PE-AuNPs (0.9 mg/ml) had a significant inhibitory effect on the

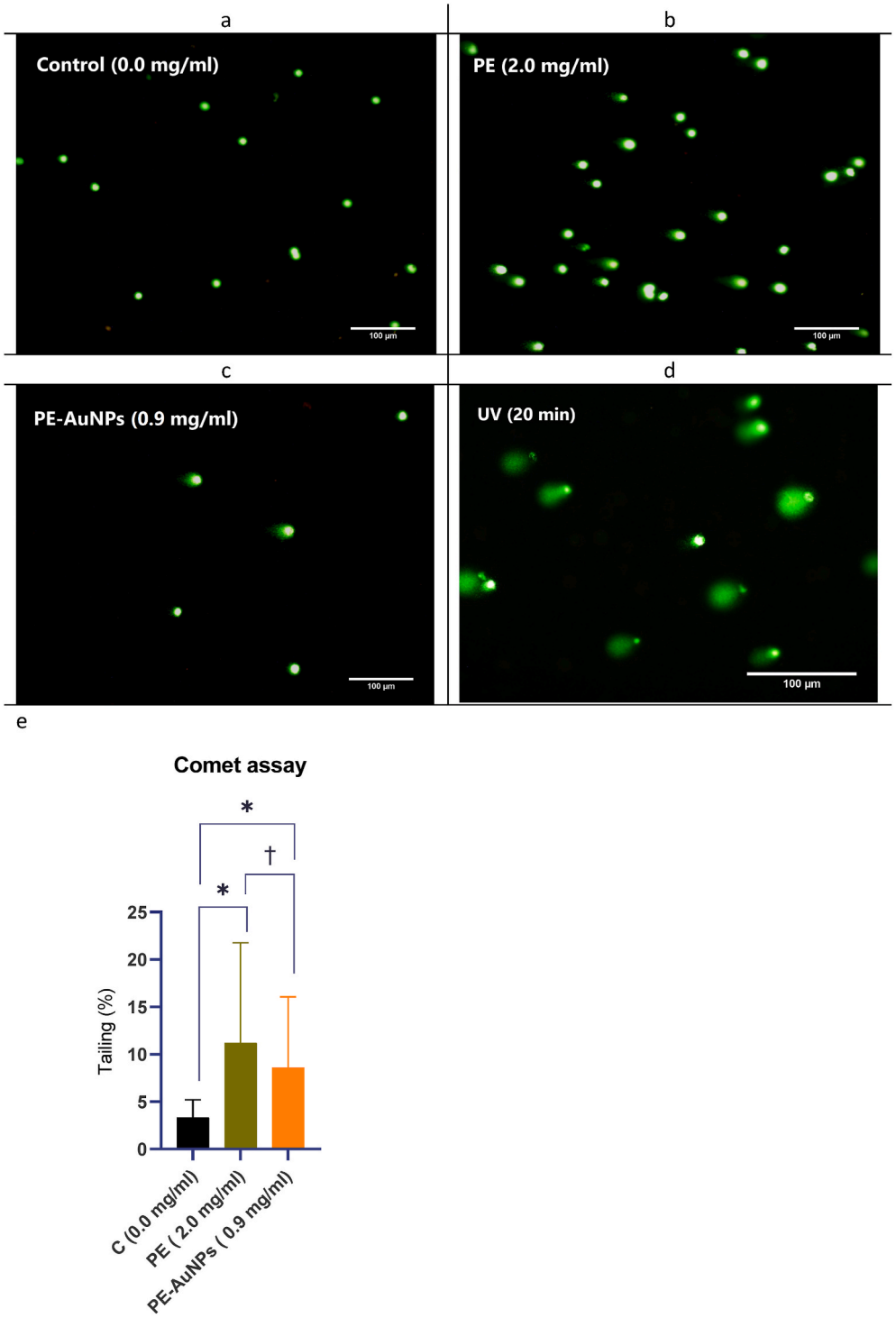

Fig. 7. The comet test. The fluorescent microscope photos depict the experimental conditions for Control (a), cells treated with MTT_{50} doses of PE (2.0 mg/ml, b) and PE-AuNPs (0.9 mg/ml, c), and UV-exposed cells (d). Additionally, the percentage of DNA tailing is shown in chart (e). †, $p < 0.05$; and *, $p < 0.0001$ compared to control (C). The data is presented as the mean ± standard deviation. The magnification is 20 × .

hatching of Artemia Salina shrimp eggs. Simultaneously, PE exhibited greater toxicity compared to PE-AuNPs. The LC_{50} values for PE and PE-AuNPs were estimated to be 1.48 $x10^3$ and 1.15 × 10^3 ppm (µg/ml), respectively, based on the percentage declines in hatching. Thus, as substances with LC_{50} values exceeding 1000 ppm are not deemed to have potential pharmacological activity [39], it may be

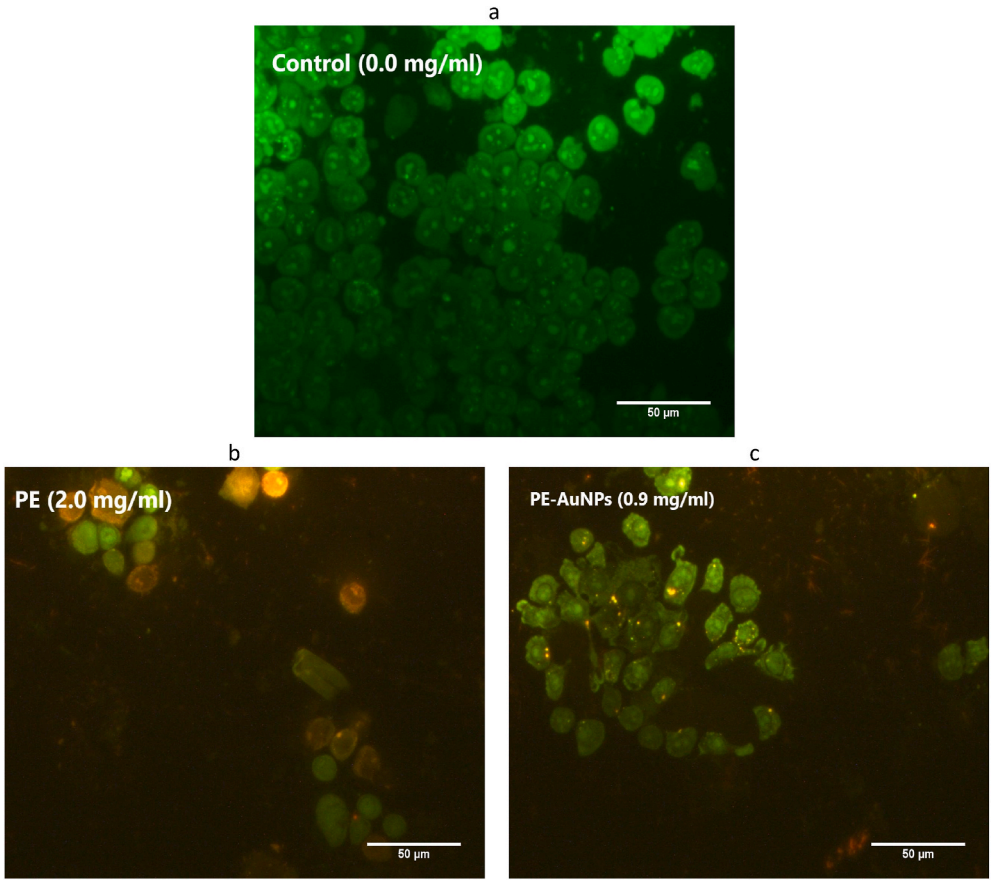

Fig. 8. The assessment of apoptosis using AO/EB double labeling. The fluorescent microscope images depict the control group (a) and cells subjected to MTT_{50} doses of PE (b) and PE-AuNPs (c) for 24 h. The magnification is 40 × .

Table 4
Apoptosis assay for *C. colocynthis* ethanolic pulp extract and the corresponding PE-AuNPs.

Sample (mg/ml)	No Apoptosis (%)	Early Apoptosis (%)	Late Apoptosis (%)	Necrosis (%)
Control	99.60 ± 0.28	0.39 ± 0.28	None	None
PE (2.0)	79.03 ± 1.82[a]	14.96 ± 1.77[a]	6.0 ± 0.04 ╪	None
PE-AuNPs (0.9)	83.80 ± 2.81[a]	15.5 ± 2.45[a]	0.69 ± 0.36	None

╪, $p < 0.001$; and.
[a] , $p < 0.0001$ compared to control, C. Data are presented as mean ± SD.

concluded that PE and PE-AuNPs are safe.

4. Discussion

Gold nanoparticles (AuNPs) were effectively synthesized through by the ethanolic extract of *C. colocynthis* pulp (PE), employing a one-step, environmentally friendly, and economically viable method for NP synthesis. Following the introduction of PE into the gold solution, the observed alteration in color from yellow to a deep purple hue served as an indication of the existence of AuNPs inside the solution. The reduction of Au^{+3} to Au^{0} was facilitated by the reducing agents in the extract. The phytochemicals present in the extract acted as both reducing and stabilizing (capping) agents during the synthesis of PE-AuNPs. Nanoparticles were synthesized using various concentrations of PE (1, 3, 6, 9, 12 mg/ml). However, the yield and size of the nanoparticles were found to be dependent on the concentration of the extract and $HAuCl_4.3H_2O$. The peak absorption exhibited a concentration-dependent increase, with higher concentrations of both $HAuCl_4.3H_2O$ and extract causing a redshift in the wavelength of λ_{max}. This shift was indicative of larger nanoparticles [1,40,41]. The initiation and completion rates of the reaction exhibited an upward trend as the concentrations of the extract were raised. Nevertheless, the reaction rate was shown to decrease as the concentration of $HAuCl_4.3H_2O$ was increased (Fig. 1). A separate investigation examined the production of AuNPs using different concentrations (0.51 mM–4.055 mM) of gold ions (Au^{+3}).

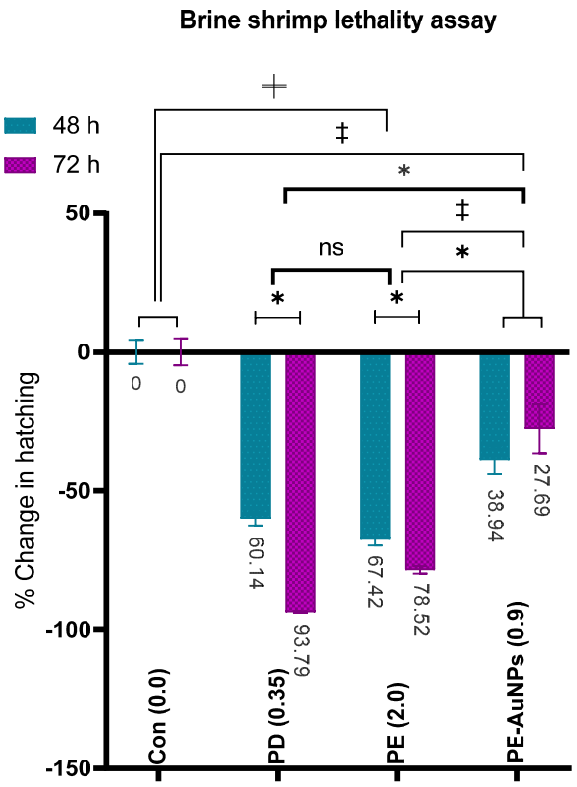

Fig. 9. Brine shrimp lethality assay. ‡, $p < 0.01$; ╪, $p < 0.001$ *, $p < 0.0001$ compared to control (C).

The results revealed that no AuNPs were formed when the Au^{+3} concentration was below 1.53 mM [42]. The results of this study suggest that the synthesis pathways or mechanisms were influenced by varying concentrations of $HAuCl_4.3H_2O$. Additional research is required to elucidate that.

Upon measurements of total phenolic content (TPC) and total antioxidant capacity (TAC) in extracts, supernatants, and AuNPs, a notable disparity in antioxidant potency was observed between the extracts and supernatants. The utilization of phytochemicals (present in PE) for nanoparticle synthesis was demonstrated by the decrease in antioxidant content in the supernatant, the identification of functional groups resembling the extract on the surface of the nanoparticles through FTIR, and the results of EDS, and TGA analyses (Table 1, Suppl. S1 and S3, and Figs. 3 and 5). However, consistent with previous research, the biosynthesized PE-AuNPs exhibited diminished antioxidant activity in comparison to PE [43]. This observation may be attributed to the adsorption of phytochemicals onto the nanoparticle surface.

Numerous studies have provided empirical evidence supporting the efficacy of gold nanoparticles as effective anticancer agents against a range of cancer cell lines, including bladder (T24) and prostate (PC-3) cancers [37,44], breast (AMJ 13 and MCF7), lung (A549), colon (HCT-15), liver (HepG2), thyroid (SW579), and colorectal adenocarcinoma cells (HT-29) [45–47]. The anticancer characteristics of gold nanoparticles are attributed to three widely acknowledged mechanisms: cell membrane damage and mitochondrial failure, formation of reactive oxygen species (ROS) and DNA fragmentation, and interference with protein/DNA chemistry.

The utilization of AuNPs in cancer treatment has been associated with little adverse effects and cytotoxicity towards healthy cells [48]. In the present investigation, it was observed that PE-AuNPs exhibited cytotoxic properties on HepG2 cells at lower doses compared to PE. This study provides more evidence in line with prior research conducted by Chang et al. (2021) [49], which documented the 48-h IC_{50} values of Cannabis sativa leaf extract and its AuNPs as 535 and 329 μg/ml against the MOLT-3 cell line, and 673 and 381 μg/ml against the TALL-104 cell line, respectively. Silver nanoparticles produced from aqueous extracts of *C. colocynthis* exhibited significant anticancer properties in HCT-116, MCF-7, Hep-G2, and Caco-2 cell lines, as compared to the aqueous extracts of the plant [50]. Hoshyar et al. demonstrated that the application of crocin-AuNPs at elevated concentrations (>2.7 mg/ml) resulted in the release of LDH from MCF-7 cells [51]. A link between the morphology of particles and the release of LDH, which acts as a signal of membrane damage, can be established. Nanoparticles have distinct shapes that result in unique properties, facilitating a broad spectrum of applications [52]. During our inspection, the scanning electron microscope identified many morphologies, including nail-like structures with a rod-shaped appearance. These rods possess the potential to penetrate cell membranes, therefore aiding in the

liberation of LDH.

The present study was conducted to assess the occurrence of apoptotic cell death in cells following exposure to PE and PE-AuNPs. In the context of fluorescence microscopy, it was shown that control cells exhibited undamaged DNA and nuclear membranes, leading to the manifestation of a brilliant green hue. On the other hand, the cells that underwent treatment exhibited early apoptosis characterized by the presence of green granulation within the cells, while late apoptosis was indicated by the emission of orange fluorescence. The findings of this study indicate that both PE and PE-AuNPs can trigger apoptosis in HepG2 cells at the IC_{50} concentration. *Enterococcus* sp.-synthesized AuNPs have also been shown to exhibit cytotoxic effects against the HepG2 cell line and to be extremely efficient in causing apoptosis [53].

Several studies have demonstrated the genotoxicity of AuNPs [9,54,55]. The alkaline comet test and micronucleus assay were conducted to assess DNA damage in cells treated with MTT_{50} concentrations of PE and PE-AuNPs. While the comet assay permits the quantification of a tested agent's direct DNA-strand breaking capacity, the MN test allows for the estimation of the induced number of chromosome and genome mutations. Our results showed that PE-AuNPs and PE caused significant DNA damage in HepG2 cells. The possibility of small nanoparticles (NPs) directly interacting with DNA by traversing the nuclear membrane is improbable in this context because the size of nuclear pores is smaller than 8 nm [56]. However, NPs can induce DNA damage by contact with DNA during mitosis when the nuclear membrane disappears [57]. Another mechanism that causes DNA damage is the release of DNase from the lysosome due to lysosomal membrane disruption by NPs [58]. Govindaraju et al. [59] conducted a biosynthesis of AuNPs utilizing Pongammia pinnata (pongam) leaf extract. The genotoxicity of these AuNPs was assessed through a comet test. The researchers demonstrated that the IC_{50} concentration of AuNPs resulted in an elongated DNA tail in MCF-7 cells as compared to cells that were not treated.

PE-AuNPs exhibited greater cytotoxicity than PE against HepG2 cells, as evidenced by a lower IC50 in MTT and NRU assays and lower viability of cells in the Trypan blue staining test. Conversely, PE resulted in a more pronounced decrease in the hatching % of brine shrimp eggs. PE-AuNPs exhibited notable DNA damage in HepG2 cells at lower IC50 concentrations compared to PE, as shown by comet and micronucleus assays. Additional research is necessary to ascertain the precise mechanism by which PE-AuNPs exert their effects. However, it appears that PE-AuNPs exhibit superior anticancer properties against HepG2 cells compared to PE.

5. Conclusion

The work effectively achieved the green synthesis of AuNPs by utilizing *C. colocynthis* in conjunction with an ethanolic extract derived from its pulp. The components derived from pulp extract were utilized as reducing and stabilizing agents in the synthesis of AuNPs. The extract's antioxidants facilitated the bioreduction of Au^{+3} to Au^{0}. The capping phytochemicals in the extract allowed the biologically produced nanoparticles to be nearly stable, as demonstrated by the TEM, DLS, agarose gel electrophoresis, and UV-VIS spectra. The cytotoxicity, genotoxicity, and apoptosis of synthesized AuNPs were seen at lower IC_{50} values in HepG2 cells compared to the crude extract. Nevertheless, the crude extract exhibited superior antioxidant properties compared to the AuNPs, effectively inhibiting the hatching of brine shrimp. Gold nanoparticles produced from the ethanolic extract of *C. colocynthis* pulp can be utilized in hepatocarcinoma treatment, provided that they are approved through in vivo tests and clinical trials.

The findings of our study indicate that the characteristics of PE-AuNPs differed from those of PE. Hence it is crucial to systematically analyze and perform toxicity assessments on the recently produced nanomaterials to ascertain their suitable application. Additional research endeavors could encompass assessing regulated cell death (RCD) mechanisms induced by nanomaterials, to establish universally accepted screening techniques to evaluate the safety of newly developed nanomaterials. Given the absence of antioxidant activity in PE-AuNPs, investigating the inflammation and ROS generation in the cells exposed to them should yield further insight into their harmful properties. Additionally, it would be intriguing to examine the chemical and physical transformations of PE-AuNPs upon their introduction into natural environments and their interaction with biomolecules. The investigation of the antidiabetic qualities and effects of PE-AuNPs would also be of interest, considering the antidiabetic nature of bitter apple.

Funding

The research was financially supported by Tehran University of Medical Sciences and Health Services, Tehran, Iran, through grant number 1400-2-101-58736.

Additional resources

This article is accompanied by four supplemental materials, denoted as S1–S4.

Data availability statement

The data will be provided upon request.

CRediT authorship contribution statement

Abbas Talebi Tadi: Writing – original draft, Investigation, Data curation. **Masoumeh Farhadiannezhad:** Methodology, Investigation, Conceptualization. **Maryam Sadat Nezamtaheri:** Validation, Methodology, Data curation. **Bahram Goliaei:** Validation, Supervision, Resources, Project administration, Methodology, Investigation. **Azin Nowrouzi:** Writing – review & editing,

Visualization, Validation, Supervision, Resources, Project administration, Methodology, Investigation, Funding acquisition, Formal analysis, Data curation, Conceptualization.

Declaration of competing interest

The authors declare that they have no known competing financial interests or personal relationships that could have appeared to influence the work reported in this paper.

Acknowledgments

The Ethical Committee of Tehran University of Medical Sciences approved this study, with the protocol code IR.TUMS.MEDICINE.REC.1401.308. The authors express their gratitude to Sharif University of Technology for generously conducting studies involving TEM, SEM, EDS, XRD, TGA, DLS, and Zeta potential. This article is the outcome of the Master of Science thesis conducted by the first author.

Appendix A. Supplementary data

Supplementary data to this article can be found online at https://doi.org/10.1016/j.heliyon.2024.e35825.

References

[1] B. Mubeen, M.G. Rasool, I. Ullah, R. Rasool, S.S. Imam, S. Alshehri, M.M. Ghoneim, S.I. Alzarea, M.S. Nadeem, I. Kazmi, Phytochemicals mediated synthesis of AuNPs from Citrullus colocynthis and their characterization, Molecules 27 (4) (2022), https://doi.org/10.3390/molecules27041300.
[2] B.H. Kiani, Q. Ajmal, N. Akhtar, I.U. Haq, M.A. Abdel-Maksoud, A. Malik, M. Aufy, N. Ullah, Biogenic synthesis of zinc oxide nanoparticles using Citrullus colocynthis for potential biomedical applications, Plants 12 (2) (2023), https://doi.org/10.3390/plants12020362.
[3] M.K.Y. Soliman, S.S. Salem, M. Abu-Elghait, M.S. Azab, Biosynthesis of silver and gold nanoparticles and their efficacy towards antibacterial, antibiofilm, cytotoxicity, and antioxidant activities, Appl. Biochem. Biotechnol. 195 (2) (2023) 1158–1183, https://doi.org/10.1007/s12010-022-04199-7.
[4] M. Kus-Liśkiewicz, P. Fickers, I. Ben Tahar, Biocompatibility and cytotoxicity of gold nanoparticles: recent advances in methodologies and regulations, Int. J. Mol. Sci. 22 (20) (2021), https://doi.org/10.3390/ijms222010952.
[5] A.A. Yaqoob, H. Ahmad, T. Parveen, A. Ahmad, M. Oves, I.M.I. Ismail, H.A. Qari, K. Umar, M.N. Mohamad Ibrahim, Recent advances in metal decorated nanomaterials and their various biological applications: a review, Front. Chem. 8 (2020), https://doi.org/10.3389/fchem.2020.00341.
[6] V. Chandrakala, V. Aruna, G. Angajala, Review on metal nanoparticles as nanocarriers: current challenges and perspectives in drug delivery systems, Emergent Mater 5 (6) (2022) 1593–1615, https://doi.org/10.1007/s42247-021-00335-x.
[7] S. Kumar, B. Kumar, R. Sehgal, M.F. Wani, D. Kumar, M.D. Sharma, V. Singh, R. Sehgal, V. Kumar, Advantages and disadvantages of metal nanoparticles, in: S. K. Tiwari, V. Kumar, S. Thomas (Eds.), Nanoparticles Reinforced Metal Nanocomposites: Mechanical Performance and Durability, Springer Nature Singapore, Singapore, 2023, pp. 209–235, https://doi.org/10.1007/978-981-19-9729-7_7.
[8] T.P. Patil, A.A. Vibhute, S.L. Patil, T.D. Dongale, A.P. Tiwari, Green synthesis of gold nanoparticles via Capsicum annum fruit extract: characterization, antiangiogenic, antioxidant and anti-inflammatory activities, Appl Surf Sci Adv 13 (2023) 100372, https://doi.org/10.1016/j.apsadv.2023.100372.
[9] Q. Xia, H. Li, Y. Liu, S. Zhang, Q. Feng, K. Xiao, The effect of particle size on the genotoxicity of gold nanoparticles, J. Biomed. Mater. Res. 105 (3) (2017) 710–719, https://doi.org/10.1002/jbm.a.35944.
[10] J. Lebedová, Y.S. Hedberg, I. Odnevall Wallinder, H.L. Karlsson, Size-dependent genotoxicity of silver, gold and platinum nanoparticles studied using the mini-gel comet assay and micronucleus scoring with flow cytometry, Mutagenesis 33 (1) (2018) 77–85, https://doi.org/10.1093/mutage/gex027.
[11] M.Z. Tan, Biosynthesis and Characterization of Gold Nanoparticles by Using Vernonia Amygdalina, Pandanus Amaryllifolius, and Citrus Maxima Leaves, UTAR, 2019. http://eprints.utar.edu.my/id/eprint/3885.
[12] P. Debnath, A. Mondal, A. Hajra, C. Das, N.K. Mondal, Cytogenetic effects of silver and gold nanoparticles on Allium cepa roots, J. Genet. Eng. Biotechnol. 16 (2) (2018) 519–526, https://doi.org/10.1016/j.jgeb.2018.07.007.
[13] S. Bawazeer, I. Khan, A. Rauf, A. Aljohani, F. Alhumaydhi, A.A. Khalil, M.N. Qureshi, L. Ahmad, S. Khan, Black pepper (Piper nigrum) fruit-based gold nanoparticles (BP-AuNPs): synthesis, characterization, biological activities, and catalytic applications-A green approach, Green Process. Synth. 11 (2022), https://doi.org/10.1515/gps-2022-0002.
[14] M.P. Patil, E. Bayaraa, P. Subedi, L.L.A. Piad, N.H. Tarte, G.-D. Kim, Biogenic synthesis, characterization of gold nanoparticles using Lonicera japonica and their anticancer activity on HeLa cells, J. Drug Deliv. Sci. Technol. 51 (2019) 83–90.
[15] A.M. Abdelghany, E.M. Abdelrazek, S.I. Badr, M.S. Abdel-Aziz, M.A. Morsi, Effect of Gamma-irradiation on biosynthesized gold nanoparticles using Chenopodium murale leaf extract, J. Saudi Chem. Soc. 21 (5) (2017) 528–537, https://doi.org/10.1016/j.jscs.2015.10.002.
[16] F.A. Alhumaydhi, I. Khan, A. Rauf, M.N. Qureshi, A.S.M. Aljohani, S.A. Khan, A.A. Khalil, M.A. El-Esawi, N. Muhammad, Synthesis, characterization, biological activities, and catalytic applications of alcoholic extract of saffron (Crocus sativus) flower stigma-based gold nanoparticles, Green Process. Synth. 10 (1) (2021) 230–245, https://doi.org/10.1515/gps-2021-0024.
[17] Z. Abootorabi, M. Poorgholami, M.Y. Hanafi-Bojd, R. Hoshyar, Green synthesis of gold nanoparticles using barberry and saffron extracts, Model. Care J 13 (4) (2016) e13000, https://doi.org/10.5812/modernc.13000.
[18] N.K.R. Bogireddy, U. Pal, L.M. Gomez, V. Agarwal, Size controlled green synthesis of gold nanoparticles using Coffea arabica seed extract and their catalytic performance in 4-nitrophenol reduction, RSC Adv. 8 (44) (2018) 24819–24826, https://doi.org/10.1039/C8RA04332A.
[19] M.L. Anitha, J. Riya, J. Rinita, P.C. Eunice, N.N. Jothi, Facile green synthesis and characterisation of gold nanoparticles using Fenugreek seeds and honey. Journal of Physics: Conference Series, IOP Publishing, 2021 012048, https://doi.org/10.1088/1742-6596/2070/1/012048.
[20] A. Afshari, F. Salimi, A. Nowrouzi, M.B. Khalili, S. Bakhtiyari, G. Hassanzadeh, M. Shabani, A. Ahadi, M. Farhadiannezhad, Differential expression of gluconeogenic enzymes in early- and late-stage diabetes: the effect of Citrullus colocynthis (L.) Schrad. Seed extract on hyperglycemia and hyperlipidemia in Wistar-Albino rats model, Clin Phytoscience 7 (1) (2021) 88, https://doi.org/10.1186/s40816-021-00324-x.
[21] M.H. Al-Ardi, The uses of gold nanoparticles and Citrullus colocynthis L. nanoparticles against Giardia lamblia in vivo, Clin Epidemiol Global Health 8 (4) (2020) 1282–1286, https://doi.org/10.1016/j.cegh.2020.04.028.
[22] H.M.H. Salama, Alkaloids and flavonoids from the air dried aerial parts of Citrullus colocynthis, J. Med. Plants Res. 6 (2012) 5150–5155, https://doi.org/10.5897/JMPR12.406.

[23] X. Chen, J. Bao, J. Guo, Q. Ding, J. Lu, M. Huang, Y. Wang, Biological activities and potential molecular targets of cucurbitacins: a focus on cancer, Anti Cancer Drugs 23 (8) (2012) 777–787, https://doi.org/10.1097/CAD.0b013e3283541384.

[24] R. Hafeez, Z. Kanwal, M.A. Raza, S. Rasool, S. Riaz, S. Naseem, S. Rabani, I. Haider, N. Ahmad, S.Y. Alomar, Role of Citrullus colocynthis and Psidium guajava mediated green synthesized silver nanoparticles in disease resistance against Aeromonas hydrophila challenge in Labeo rohita, Biomedicines (2023), https://doi.org/10.3390/biomedicines11092349.

[25] H.O. Ibrahim, H.T. Taha, R.T. Ali, Green synthesis of copper nanoparticles using Citrullus colocynthis peel extract and antibacterial activity for biomedical applications, ECS J Solid State Sci Technol 12 (10) (2023) 101003, https://doi.org/10.1149/2162-8777/acff84.

[26] S. Karunakaran, R. Hari, Comparative antioxidant and anti-gout activities of Citrullus colocynthis loaded fruit silver nanoparticles with its ethanolic extract, Avicenna J. Med. Biotechnol. (AJMB) 14 (4) (2022) 303–309. https://www.ncbi.nlm.nih.gov/pubmed/36504570.

[27] S. Kiran, M.A. Rafique, S. Iqbal, S. Nosheen, S. Naz, A. Rasheed, Synthesis of nickel nanoparticles using Citrullus colocynthis stem extract for remediation of Reactive Yellow 160 dye, Environ. Sci. Pollut. Res. Int. 27 (26) (2020) 32998–33007, https://doi.org/10.1007/s11356-020-09510-9.

[28] S. Rasool, A. Tayyeb, M.A. Raza, H. Ashfaq, S. Perveen, Z. Kanwal, S. Riaz, S. Naseem, N. Abbas, N. Ahmad, S.Y. Alomar, Citrullus colocynthis-mediated green synthesis of silver nanoparticles and their antiproliferative action against breast cancer cells and bactericidal roles against human pathogens, Nanomaterials 12 (21) (2022), https://doi.org/10.3390/nano12213781.

[29] B. Hameed, A. Cd, M. Hafeez, A. Malik, Antibacterial and antifungal activity of fruit, seed and root extracts of Citrullus colocynthis plant, Biol Clin Sci Res J (2020) 1–5, https://doi.org/10.47264/bcsrj0101033, 2020.

[30] N. Torabi, A. Nowrouzi, A. Ahadi, S. Vardasbi, B. Etesami, Green synthesis of gold nanoclusters using seed aqueous extract of Cichorium intybus L. and their characterization, SN Appl. Sci. 1 (9) (2019) 1–14, https://doi.org/10.1007/s42452-019-1035-x.

[31] E. Borenfreund, J.A. Puerner, A simple quantitative procedure using monolayer cultures for cytotoxicity assays (HTD/NR-90), J. Tissue Cult. Methods 9 (1) (1985) 7–9, https://doi.org/10.1007/BF01666038.

[32] E. Nowak, S. Kammerer, J.H. Küpper, ATP-based cell viability assay is superior to trypan blue exclusion and XTT assay in measuring cytotoxicity of anticancer drugs Taxol and Imatinib, and proteasome inhibitor MG-132 on human hepatoma cell line HepG2, Clin. Hemorheol. Microcirc. 69 (1–2) (2018) 327–336, https://doi.org/10.3233/ch-189120.

[33] B. Bigdeli, B. Goliaei, N. Masoudi-Khoram, N. Jooyan, A. Nikoofar, M. Rouhani, A. Haghparast, F. Mamashli, Enterolactone: a novel radiosensitizer for human breast cancer cell lines through impaired DNA repair and increased apoptosis, Toxicol. Appl. Pharmacol. 313 (2016) 180–194, https://doi.org/10.1016/j.taap.2016.10.021.

[34] T.B. Queiroz, G.F. Santos, S.C. Ventura, C.A. Hiruma-Lima, I.O.M. Gaivão, E.L. Maistro, Cytotoxic and genotoxic potential of geraniol in peripheral blood mononuclear cells and human hepatoma cell line (HepG2), Genet. Mol. Res. 16 (3) (2017), https://doi.org/10.4238/gmr16039777.

[35] J. Zhao, Y. Wu, A.T. Alfred, P. Wei, S. Yang, Anticancer effects of pyocyanin on HepG2 human hepatoma cells, Lett. Appl. Microbiol. 58 (6) (2014) 541–548, https://doi.org/10.1111/lam.12224.

[36] J. Kapali, K.R. Sharma, Estimation of phytochemicals, antioxidant, antidiabetic and brine shrimp lethality activities of some medicinal plants growing in Nepal, J Medicinal Plants 20 (80) (2021) 102–116, https://doi.org/10.52547/jmp.20.80.102.

[37] C.E.A. Botteon, L.B. Silva, G.V. Ccana-Ccapatinta, T.S. Silva, S.R. Ambrosio, R.C.S. Veneziani, J.K. Bastos, P.D. Marcato, Biosynthesis and characterization of gold nanoparticles using Brazilian red propolis and evaluation of its antimicrobial and anticancer activities, Sci. Rep. 11 (1) (2021) 1974, https://doi.org/10.1038/s41598-021-81281-w.

[38] A. Avalos, A.I. Haza, D. Mateo, P. Morales, In vitro and in vivo genotoxicity assessment of gold nanoparticles of different sizes by comet and SMART assays, Food Chem. Toxicol. 120 (2018) 81–88, https://doi.org/10.1016/j.fct.2018.06.061.

[39] K.R. Sharma, R. Kharel, Antibacterial, antidiabetic and brine shrimp lethality activities of some selected medicinal plants from Kavrepalanchok District of Nepal, Journal of Institute of Science and Technology 24 (1) (2019) 57–62, https://doi.org/10.3126/jist.v24i1.24629.

[40] T. Ahmad, M. Irfan, S. Bhattacharjee, Parametric study on gold nanoparticle synthesis using aqueous Elaise Guineensis (Oil palm) leaf extract: effect of precursor concentration, Procedia Eng. 148 (2016) 1396–1401, https://doi.org/10.1016/j.proeng.2016.06.558.

[41] H.S. Kim, D.Y. Lee, Near-infrared-responsive cancer photothermal and photodynamic therapy using gold nanoparticles, Polymers 10 (9) (2018), https://doi.org/10.3390/polym10090961.

[42] A.R. Shafiqa, A. Abdul Aziz, B. Mehrdel, Nanoparticle optical properties: size dependence of a single gold spherical nanoparticle, J. Phys. Conf. 1083 (2018) 012040, https://doi.org/10.1088/1742-6596/1083/1/012040.

[43] S.O. Anadozie, O.B. Adewale, M. Meyer, H. Davids, S. Roux, In vitroanti-oxidant and cytotoxic activities of gold nanoparticles synthesized from an aqueous extract of theXylopia aethiopicafruit, Nanotechnology 32 (31) (2021), https://doi.org/10.1088/1361-6528/abf6ee.

[44] T. Wu, X. Duan, C. Hu, C. Wu, X. Chen, J. Huang, J. Liu, S. Cui, Synthesis and characterization of gold nanoparticles from Abies spectabilis extract and its anticancer activity on bladder cancer T24 cells, Artif. Cells, Nanomed. Biotechnol. 47 (1) (2019) 512–523, https://doi.org/10.1080/21691401.2018.1560305.

[45] K.D. Datkhile, S.R. Patil, P.P. Durgawale, M.N. Patil, D.D. Hinge, N.J. Jagdale, V.N. Deshmukh, A.L. More, Biogenic synthesis of gold nanoparticles using Argemone mexicana L. and their cytotoxic and genotoxic effects on human colon cancer cell line (HCT-15), J. Genet. Eng. Biotechnol. 19 (1) (2021) 9, https://doi.org/10.1186/s43141-020-00113-y.

[46] K. Perveen, F.M. Husain, F.A. Qais, A. Khan, S. Razak, T. Afsar, P. Alam, A.M. Almajwal, M.M.A. Abulmeaty, Microwave-assisted rapid green synthesis of gold nanoparticles using seed extract of Trachyspermum ammi: ROS mediated biofilm inhibition and anticancer activity, Biomolecules (2021), https://doi.org/10.3390/biom11020197.

[47] R.M. Yas, A. Ghafoor, M.A. Saeed, Anticancer effect of green synthesized gold nanoparticles using orchid extract and their characterizations on breast cancer AMJ-13 Cell line, Sys. Rev. Pharm. 12 (2021) 500–505, https://doi.org/10.31838/srp.2021.2.68.

[48] K.K. Bharadwaj, B. Rabha, S. Pati, T. Sarkar, B.K. Choudhury, A. Barman, D. Bhattacharjya, A. Srivastava, D. Baishya, H.A. Edinur, Z. Abdul Kari, N.H. Mohd Noor, Green synthesis of gold nanoparticles using plant extracts as beneficial prospect for cancer theranostics, Molecules 26 (21) (2021), https://doi.org/10.3390/molecules26216389.

[49] Y. Chang, C. Zheng, A. Chinnathambi, T.A. Alahmadi, S.A. Alharbi, Cytotoxicity, anti-acute leukemia, and antioxidant properties of gold nanoparticles green-synthesized using Cannabis sativa L leaf aqueous extract, Arab. J. Chem. 14 (4) (2021) 103060, https://doi.org/10.1016/j.arabjc.2021.103060.

[50] A.M. Shawkey, M. Rabeh, A. Abdulall, A.O. Abdellatif, Green nanotechnology: anticancer activity of silver nanoparticles using Citrullus colocynthis aqueous extracts, Adv. Life Sci. Technol. 13 (2013) 60–70.

[51] R. Hoshyar, G.R. Khayati, M. Poorgholami, M. Kaykhaii, A novel green one-step synthesis of gold nanoparticles using crocin and their anti-cancer activities, J. Photochem. Photobiol. B Biol. 159 (2016) 237–242, https://doi.org/10.1016/j.jphotobiol.2016.03.056.

[52] M.M. Ghobashy, S.A. Alkhursani, H.A. Alqahtani, T.K. El-damhougy, M. Madani, Gold nanoparticles in microelectronics advancements and biomedical applications, Mater. Sci. Eng., B 301 (2024) 117191, https://doi.org/10.1016/j.mseb.2024.117191.

[53] J. Nandhini, E. Devaraj, R. Shanmugam, An ecofriendly synthesized gold nanoparticles induces cytotoxicity via apoptosis in HepG2 cells, Environ. Toxicol. 36 (2020), https://doi.org/10.1002/tox.23007.

[54] A. Parveen, S. Rao, Cytotoxicity and genotoxicity of biosynthesized gold and silver nanoparticles on human cancer cell lines, J. Cluster Sci. 26 (2015) 775–788.

[55] M. Uzma, N. Sunayana, V.B. Raghavendra, C.S. Madhu, R. Shanmuganathan, K. Brindhadevi, Biogenic synthesis of gold nanoparticles using Commiphora wightii and their cytotoxic effects on breast cancer cell line (MCF-7), Process Biochem 92 (2020) 269–276, https://doi.org/10.1016/j.procbio.2020.01.019.

[56] L.J. Terry, E.B. Shows, S.R. Wente, Crossing the nuclear envelope: hierarchical regulation of nucleocytoplasmic transport, Science 318 (5855) (2007) 1412–1416, https://doi.org/10.1126/science.1142204.

[57] L. Gonzalez, D. Lison, M. Kirsch-Volders, Genotoxicity of engineered nanomaterials: a critical review, Nanotoxicology 2 (4) (2008) 252–273, https://doi.org/10.1080/17435390802464986.
[58] A. Banasik, A. Lankoff, A. Piskulak, K. Adamowska, H. Lisowska, A. Wojcik, Aluminum-induced micronuclei and apoptosis in human peripheral-blood lymphocytes treated during different phases of the cell cycle, Environ. Toxicol. 20 (4) (2005) 402–406, https://doi.org/10.1002/tox.20125.
[59] K. Govindaraju, R. Vasantharaja, K.S. Uma Suganya, S. Anbarasu, K. Revathy, A. Pugazhendhi, D. Karthickeyan, G. Singaravelu, Unveiling the anticancer and antimycobacterial potentials of bioengineered gold nanoparticles, Process Biochem 96 (2020) 213–219, https://doi.org/10.1016/j.procbio.2020.06.016.